

High-resolution angle-resolved photoemission study of oxygen adsorbed Fe/MgO(001)

Mingtian Zheng, Eike F. Schwier, Hideaki Iwasawa, Kenya Shimada

Citation: Chin. Phys. B . 2020, 29(6): 067901 . **doi:** 10.1088/1674-1056/ab9196
Journal homepage: http://cpb.iphy.ac.cn; http://iopscience.iop.org/cpb

What follows is a list of articles you may be interested in

In-situ spectroscopic studies and interfacial engineering on FeSe/oxide heterostructures: Insights on the interfacial superconductivity

Peng Rui, Xu Hai-Chao, Feng Dong-Lai

Chin. Phys. B . 2015, 24(11): 117902 . **doi:** 10.1088/1674-1056/24/11/117902

Temperature effect on the electronic structure of Nb:$SrTiO_3$ (100) surface

Zhang Shuang-Hong, Wang Jia-Ou, Qian Hai-Jie, Wu Rui, Zhang Nian, Lei Tao, Liu Chen, Kurash Ibrahim

Chin. Phys. B . 2015, 24(2): 027901 . **doi:** 10.1088/1674-1056/24/2/027901

Mn overlayers on PbTe (111): Substitutional adsorption and interface formation

Wu Hai-Fei, Zhang Han-Jie, Lu Yun-Hao, Yan Yong-Hong, Li Hai-Yang, Bao Shi-Ning, He Pi-Mo

Chin. Phys. B . 2014, 23(12): 127901 . **doi:** 10.1088/1674-1056/23/12/127901

Influence of wet chemical cleaning on quantum efficiency of GaN photocathode

Wang Xiao-Hui, Gao Pin, Wang Hong-Gang, Li Biao, Chang Ben-Kang

Chin. Phys. B . 2013, 22(2): 027901 . **doi:** 10.1088/1674-1056/22/2/027901

The optimal thickness of transmission-mode GaN photocathode

Wang Xiao-Hui, Shi Feng, Guo Hui, Hu Cang-Lu, Cheng Hong-Chang, Chang Ben-Kang, Ren Ling, Du Yu-Jie, Zhang Jun-Ju

Chin. Phys. B . 2012, 21(8): 087901 . **doi:** 10.1088/1674-1056/21/8/087901

RAPID COMMUNICATION

High-resolution angle-resolved photoemission study of oxygen adsorbed Fe/MgO(001)

Mingtian Zheng[1,†], Eike F. Schwier[2], Hideaki Iwasawa[1,§], and Kenya Shimada[2,‡]

[1] *Graduate School of Science, Hiroshima University, Kagamiyama* 1-3-1, *Higashi-Hiroshima* 739-8526, *Japan*

[2] *Hiroshima Synchrotron Radiation Center, Hiroshima University, Kagamiyama* 2-313, *Higashi-Hiroshima* 739-0046, *Japan*

(Received 29 April 2020; revised manuscript received 9 May 2020; accepted manuscript online 11 May 2020)

We have investigated the electronic states of clean Fe(001) and oxygen adsorbed Fe(001)–$p(1\times1)$-O films epitaxially grown on MgO(001) substrates by means of polarization-dependent angle-resolved photoemission spectroscopy (ARPES) and extensive density-functional theory (DFT) calculations. The observed Fermi surfaces and band dispersions of pure Fe near the Fermi level were modified upon oxygen adsorption. By the detailed comparison of ARPES and DFT results of the oxygen adsorbed Fe surface, we have clarified the orbital-dependent p–d hybridization in the topmost and second Fe layers. Furthermore, the observed energy levels and Fermi wave numbers for the oxygen adsorbed Fe surface were deviated from the DFT calculations depending on the orbital characters and momentum directions, indicating an anisotropic interplay of the electron correlation and p–d hybridization effects in the surface region.

Keywords: angle-resolved photoemission, iron surface, oxygen adsorption, density-functional theory (DFT)

PACS: 79.60.–i, 68.47.Gh, 75.70.–i **DOI:** 10.1088/1674-1056/ab9196

1. Introduction

The metal–oxide interface is one of the most extensively investigated topics in the surface science.[1–4] The strong bonding between oxygen and metal atoms at the surface significantly modifies the crystallographic and electronic structures, which affects the transport and magnetic properties such as the tunnel magnetoresistance effect[5] as well as the catalytic reactions at the surface.[4,6] The $p(1\times1)$ oxygen adsorbed ferromagnetic Fe(001) surface is one of the prototypical systems for the metal–oxide interface and has been extensively studied for decades.[4,7–28] The adsorbed single layer oxygen atoms occupy the fourfold hollow sites of the Fe(001) surface and are situated on-top of the subsurface Fe atoms.[4] The structural studies of the Fe(001)–$p(1\times1)$-O surface using the low-energy electron diffraction (LEED) and medium-energy ion scattering measurements clarified that the spacing between the topmost and second Fe layers (d_{12}) was 1.54–1.55 Å[7,8] and 1.59 Å,[9] respectively. The obtained d_{12} was enhanced by 8%–11% compared with the bulk value 1.43 Å.[8] On the other hand, the distance between the oxygen atoms to the topmost Fe layer $d_{\mathrm{O-Fe}}$ was evaluated to be 0.45 Å.[8] Recent surface x-ray diffraction study has elucidated d_{12} to be 1.66 Å, which is 16% larger than that in the bulk and $d_{\mathrm{O-Fe}}$ is 0.48 Å.[10] The density functional theory (DFT) calculations on the oxygen adsorbed Fe surface have been carried out using a slab model.[11–15] Due to the strong bonding between the adsorbed O 2p and Fe 3d states, the d_{12} and magnetic moments of the first few Fe layers become larger than those in the bulk.[11–15] Previous angle-resolved photoemission spectroscopy (ARPES)[16–19] on Fe(001)–$p(1\times1)$-O surface clarified the O 2p-derived states in the energy range of -4 eV to -9 eV well below the Fermi level (E_{F}) and the momentum dependent exchange splitting of O 2p [1.3 (0.25) eV and 0.36 (0.20) eV for $2p_z$ and $2p_x$, respectively at the zone center ($\overline{X}$ point)].[17] The inverse photoemission spectroscopy clarified that the surface-derived minority-spin Fe $3d_{3z^2-r^2}$ state exists just above E_{F} on clean Fe(001) while the Fe $3d_{3z^2-r^2}$ surface state is quenched and an image-potential state appears on the Fe(001)–$p(1\times1)$-O surface.[20] These observations indicate enhanced spin polarization and higher electron reflectivity of the Fe(001)–$p(1\times1)$-O surface. The scanning tunneling microscopy and spectroscopy of the Fe(001)–$p(1\times1)$-O surface have provided the surface morphology as well as the local density of states (LDOS).[21–24] By comparing the observed LDOS and the theoretical calculations using a Green's-function multiple-scattering approach within DFT, the peak at -0.7 eV was derived from the hybridization between the Fe $3d_{xz}$, $3d_{yz}$ and O $2p_x$, $2p_y$ states in the topmost layer, and the peak just above E_{F} from the hybridization between the Fe $3d_{3z^2-r^2}$ and O $2p_z$ states in the subsurface layer.[24] Meanwhile, the large spin-dependent electron reflectivity and absorption of the Fe(001)–$p(1\times1)$-O surface[25–27] have been

§Present address: Synchrotron Radiation Research Center, National Institutes for Quantum and Radiological Science and Technology, 1-1-1 Kouto, Sayo, Hyogo 679-5148, Japan

†Corresponding author. E-mail: zhengmingtian@hiroshima-u.ac.jp

‡Corresponding author. E-mail: kshimada@hiroshima-u.ac.jp

© 2020 Chinese Physical Society and IOP Publishing Ltd

successfully applied to the highly efficient target materials for the very low-energy-electron-diffraction (VLEED) type spin detector.[28]

Nevertheless, quantitative investigation of the orbital characters of the energy bands near E_F in the surface region is still lacking. In addition, ferromagnetic Fe is a typical multi-band system, and the electron correlation effect depends on the orbital character and momentum direction.[29,30] From this point of view, detailed understanding of electron correlation as well as p–d hybridization of the Fe(001)–$p(1\times1)$-O surface is far from satisfactory.

In this study, we have investigated surface- and bulk-derived electronic states near E_F of the Fe(001) and Fe(001)–$p(1\times1)$-O surfaces by utilizing linear-polarization-dependent high-resolution ARPES measurements combined with state-of-the-art DFT calculations. We have provided experimental evidence for the orbital dependent hybridization between the absorbed O and Fe atoms near E_F in the surface region. These observations are further depicted by the layer- and orbital-resolved DFT calculations.

2. Density-functional theory calculation

We have done DFT calculations for a 41 monolayer (ML) thick Fe(001) slab covered with a $p(1\times1)$ O layer on both surfaces. The DFT calculations were performed using the openMX code,[31] norm-conserving scalar relativistic pseudopotentials, and pseudo-atomic localized basis functions. We used the LSDA functional as proposed by Ceperley and Alder[32] and colinear magnetism. The slab was constructed from a fully relaxed bulk Fe lattice structure and the atomic positions in the slab were subsequently relaxed with residual forces being smaller than 10^{-4} Bohr/Hartree. The adsorbed oxygen atoms occupied the hollow site of the surface. The Brillouin zone was sampled using a $24\times24\times1$ k-point mesh and the cut-off energy was 300 Ry. Soft pseudopotentials were used for Fe with a basis set chosen as $s^3p^3d^2f^1$. The O basis was set as $s^2p^2d^1$.

The slab band dispersion $E_B(k_{\|})$ along the $\overline{\Gamma}$–$\overline{X}$ and $\overline{\Gamma}$–$\overline{M}$ high symmetry lines was then calculated. Since a large number of atoms and hence electrons in the slab are involved in the DFT calculations, the resultant raw band structures are quite complex with many quantum-well-like bands that are related to the electrons contributing to the bulk bands. To discuss the electronic structures at the surface or in the bulk, it is necessary to calculate each contribution from a certain atom in the slab.

Using the unfolding procedure implemented in the openMX code,[33,34] we extracted the orbital (l,m) and spin (s) contribution of each atom (A) in the slab layer at each eigenenergy of the electron band dispersion. Then we constructed image plots showing the contributions from each atom as well as orbitals and spins by adding a Gaussian function with an area proportional to the orbital weight $I_A(l,m,s)$ to each point of the band dispersion. This method allows us to determine the orbital hybridization as well as the spin structure of the surface and more bulk-like regions deeper inside the slab.

A Mulliken charge analysis[35] was used to analyze the variation of valance of the Fe atoms as a function of position within the slab and to clarify the effect of the charge transfer in the oxygen adsorbed Fe(001) slab. We have found sizable deviation of the charge distribution in the 1st and 2nd Fe layers from that of the central Fe layer (the 21st layer counting from the surface Fe layer, which is regarded as bulk). In the current analysis, therefore, we focus on the electronic structures in the surface region, namely, O atoms at the surface, the 1st and 2nd Fe layers, and the electronic structure of the Fe layer in the bulk (central layer of the slab).

3. Experiment

Fe(001) and Fe(001)–$p(1\times1)$-O films were grown on MgO(001) substrates. Single-crystalline MgO(001) substrates (one-side polished, 7 mm×7 mm, 0.5 mm thick) were cleaned by annealing (800 K for 12 h) in an ultrahigh-vacuum chamber (base pressure: 2×10^{-10} Torr). An electron beam evaporator (EFM 3, Omicron, Germany) was used to deposit Fe on MgO(001). The thickness of the Fe film was typically $\sim$ 100 nm. A well ordered Fe(001) surface was obtained after annealing at 800 K for 30 min. In order to prepare the oxygen adsorbed surface, about 1500 L O_2 was dosed on the Fe(001) film (5×10^{-6} Torr for 5 min) at room temperature. Then the sample was heated by flash annealing to 900 K to make a uniform single monolayer of O.

The cleanness of Fe(001) and oxygen adsorbed Fe(001) surfaces was characterized by Auger electron spectroscopy and the 1×1 surface structure was confirmed by the LEED image. Figures 1(a) and 1(b) show the LEED images for pure Fe(001) and Fe(001)–$p(1\times1)$-O, respectively. A sharp 1×1 pattern clearly indicated that our sample surfaces were clean and well-ordered.

High-resolution ARPES experiments were performed on the linear-undulator beamline (BL-1) of a compact electron-storage ring (HiSOR) at Hiroshima University.[36,37] The data were obtained using the angular mode of a hemispherical electron-energy analyzer (R4000, VG-Scienta, Sweden). The analyzer chamber can be rotated around the linearly polarized light axis, which enables us to examine ARPES spectra with the p- or s-polarization geometries. In the p-polarization geometry, the vector potential which is parallel to the electric-field vector lies on the photoelectron detection plane as well as the light incidence plane. On the other hand, in the s-polarization geometry, the vector potential is perpendicular to

the detection plane. Within the free-electron final-state approximation, the initial states of even symmetry with respect to the detection plane [= mirror plane of Fe(001)] can be observed using the *p*-polarization geometry, while those having odd symmetry using the *s*-polarization geometry.[37]

All of the ARPES results shown in this study were taken at a photon energy of $h\nu = 55$ eV for enhanced surface sensitivity. With this photon energy, the bulk bands detected by the ARPES measurements in the normal emission geometry are closer to those at the Γ point of the bulk Brillouin zone.[38] The total energy resolution was set to $\Delta E = 16$ meV. The angular resolution was $\Delta\theta = 0.8^\circ$ (FWHM), which provides a momentum resolution of $\delta k = 0.051$ Å^{-1}. The sample temperature was set at 12 K during the ARPES measurements.

4. Orbital symmetry and compatibility relation

By employing a polarization-dependent ARPES experiment, we can selectively observe electronic states having even or odd symmetry with respect to the mirror plane of the sample, and directly compare the results with the DFT calculations. In this analysis, decomposition into the basis functions (xy, yz, zx, x^2-y^2, $3z^2-r^2$, x, y, z) along the high symmetry lines [$\overline{\Gamma}$–$\overline{X}$, $\overline{\Gamma}$–$\overline{M}$ in Fig. 1(c)] is useful.

Setting the mirror plane standing on the $\overline{\Gamma}$–$\overline{X}$ line ($y = 0$ or $k_y = 0$ plane), the electronic states derived from the Fe $3d_{xz}$, $3d_{x^2-y^2}$, $3d_{3z^2-r^2}$, and O $2p_x$, $2p_z$ orbitals are even because they do not change their sign under the mirror operation m_y: $y \to -y$. On the other hand, the electronic states derived from the Fe $3d_{xy}$, $3d_{yz}$, and O $2p_y$ orbitals are odd because they change their sign under the m_y operation.

If we set the mirror plane standing on the $\overline{\Gamma}$–$\overline{M}$ line ($x = y$ or $k_x = k_y$ plane), the electronic states derived from the Fe $3d_{xy}$, $3d_{(x+y)z}$, $3d_{3z^2-r^2}$, and O $2p_{x+y}$, $2p_z$ are even because they do not change their sign under the mirror operation m_d: $x \to y$ and $y \to x$. On the other hand, the electronic states derived from the Fe $3d_{(x-y)z}$, $3d_{x^2-y^2}$, and O $2p_{x-y}$ orbitals are odd because they change their sign under the m_d operation. We should note here that in the present calculations the contributions from the Fe $3d_{xz}$ and $3d_{yz}$ orbitals are identical to the energy bands along the $\overline{\Gamma}$–$\overline{M}$ line due to the symmetry property. Namely, the contribution from the Fe $3d_{(x+y)z}$ orbital is essentially the same with that from the Fe $3d_{xz}$ and $3d_{yz}$ orbitals. The situation is the same for O $2p_x$, $2p_y$, and O $2p_{x+y}$ orbitals. On the other hand, the Fe $3d_{(x-y)z}$ and O $2p_{x-y}$ contributions are vanishing because the Fe $3d_{xz}$ and $3d_{yz}$ (O $2p_x$ and $2p_y$) contributions cancel each other along the $\overline{\Gamma}$–$\overline{M}$ line.

To understand the orbital-dependent p–d hybridization near the surface region, here we consider the compatibility relation for the two-dimensional square lattice.[39] The basis functions are classified into Γ_1 ($3z^2-r^2$, z), Γ_3 (x^2-y^2), Γ_4 (xy), and Γ_5 (xz, yz, x, y) at the $\overline{\Gamma}$ point.[39] Along the Δ ($\overline{\Gamma}$–$\overline{X}$) line, Γ_1, Γ_3, and Γ_5 are compatible with the Δ_1 (+1 under the m_y operation), and Γ_4 and Γ_5 are compatible with the Δ_2 (−1 under the m_y operation).[39] Along the Σ ($\overline{\Gamma}$–$\overline{M}$) line, on the other hand, Γ_1, Γ_4, and Γ_5 are compatible with the Σ_1 (+1 under the m_d operation), and Γ_3 and Γ_5 are compatible with the Σ_2 (−1 under the m_d operation).[39] The energy bands having the same symmetry can mix with each other if the energy levels are identical along these high symmetry lines. With the *p*(*s*)-polarization geometry, we can detect Δ_1 (Δ_2) and Σ_1 (Σ_2) along the Δ (Σ) line.

In the ARPES experiments, we can also observe the bulk-derived electronic states. Near E_F, there exist the minority-spin Γ'_{25} (T_{2g}: xy, yz, zx) and majority-spin Γ_{12} (E_g: x^2-y^2, $3z^2-r^2$) bands along the Γ–H (Δ) and Γ–N (Σ) lines[40] of the bulk Brillouin zone. Note that taken at $h\nu = 55$ eV, the $\overline{\Gamma}$–$\overline{X}$ ($\overline{\Gamma}$–$\overline{M}$) line of the surface Brillouin zone is closer to the Γ–H (Γ–N) line of the bulk Brillouin zone.[38]

5. Results and discussion

Figures 1(d) and 1(e) show ARPES intensity plots near E_F of pure Fe(001) with the *p*- and *s*-polarization geometries, respectively. To clearly sort out the energy bands by the orbital symmetry, we have measured ARPES spectra along the $\overline{\Gamma}$–$\overline{X}$ and $\overline{\Gamma}$–$\overline{M}$ high symmetry lines of the surface Brillouin zone. Since there exists a strong emission-angle dependence in the spectral intensity due to the matrix element effects, we have added the ARPES intensities for the positive and negative directions with respect to the $\overline{\Gamma}$ point along the high symmetry lines. In Fig. 1(d), an electron-like band dispersion centered at the $\overline{\Gamma}$ point has its energy minimum at −0.2 eV and crossing E_F at $k_\parallel = 0.4$ Å^{-1}. A broad electron-like band centered at the $\overline{X}$ point also crosses E_F at $k_\parallel = 0.6$ Å^{-1}. Another hole-like band centered at the $\overline{X}$ point has its energy maximum near E_F. A hole-like band centered at the $\overline{\Gamma}$ point has energy maximum at −0.2 eV along the $\overline{\Gamma}$–$\overline{X}$ and $\overline{\Gamma}$–$\overline{M}$ lines. Around the $\overline{M}$ point, a hole-like band is crossing E_F at $k_\parallel = 1.18$ Å^{-1} and a broad feature exists around −0.5 eV. Figure 1(e) shows that around the $\overline{\Gamma}$ point electron-like bands with energy minimum at −0.2 eV are crossing E_F along the $\overline{\Gamma}$–$\overline{X}$ and $\overline{\Gamma}$–$\overline{M}$ lines as well as hole-like bands exist just below the energy of −0.2 eV. Moreover, around the $\overline{X}$ point, a hole-like band crosses E_F, which is distinct from the spectral feature in the *p*-polarization geometry [Fig. 1(d)], suggesting two hole-like Fermi surfaces near the $\overline{X}$ point.

Figures 1(f) and 1(g) show the ARPES intensity plots of Fe(001)–$p(1\times1)$-O with the *p*- and *s*-polarization geometries, respectively. It is clearly seen that the spectral line widths become narrower after the oxygen adsorption. In Fig. 1(f), along the $\overline{\Gamma}$–$\overline{X}$ line, electron-like bands I_a and I_b are crossing E_F, and another band VI lies between −0.25 eV and E_F. Moreover,

there exist a hole-like broad band IX having the energy maximum of −0.2 eV at the $\overline{\Gamma}$ point and a hole-like band XI centered at the $\overline{X}$ point. Along the $\overline{\Gamma}$–$\overline{M}$ line, on the other hand, electron-like bands II and III are crossing E_F around $k_{\|} = 0.3$–0.4 Å^{-1}. A hole-like band X exists below bands II and III with the energy maximum at −0.2 eV at the $\overline{\Gamma}$ point. A hole-like band VIII is crossing E_F at $k_{\|} = 1.23$ Å^{-1}, which is similar to the pure Fe in Fig. 1(d). The energy band VII newly appears between band III and band VIII, and a hole-like band XII with a flat portion at about −0.45 eV around the $\overline{M}$ point. In Fig. 1(g), along the $\overline{\Gamma}$–$\overline{X}$ line, electron-like bands VI_a and VI_b are crossing E_F, and a hole-like band XIII exists with the energy maximum at −0.2 eV at the $\overline{\Gamma}$ point. Moreover, there exists a hole-like broad band XV having the energy maximum of −0.4 eV at the $\overline{X}$ point. A broad feature XVI approaching to E_F around the $\overline{X}$ point is also discernible. Along the $\overline{\Gamma}$–$\overline{M}$ line, an electron-like band V is crossing E_F and a hole-like band XIV exists at the $\overline{\Gamma}$ point.

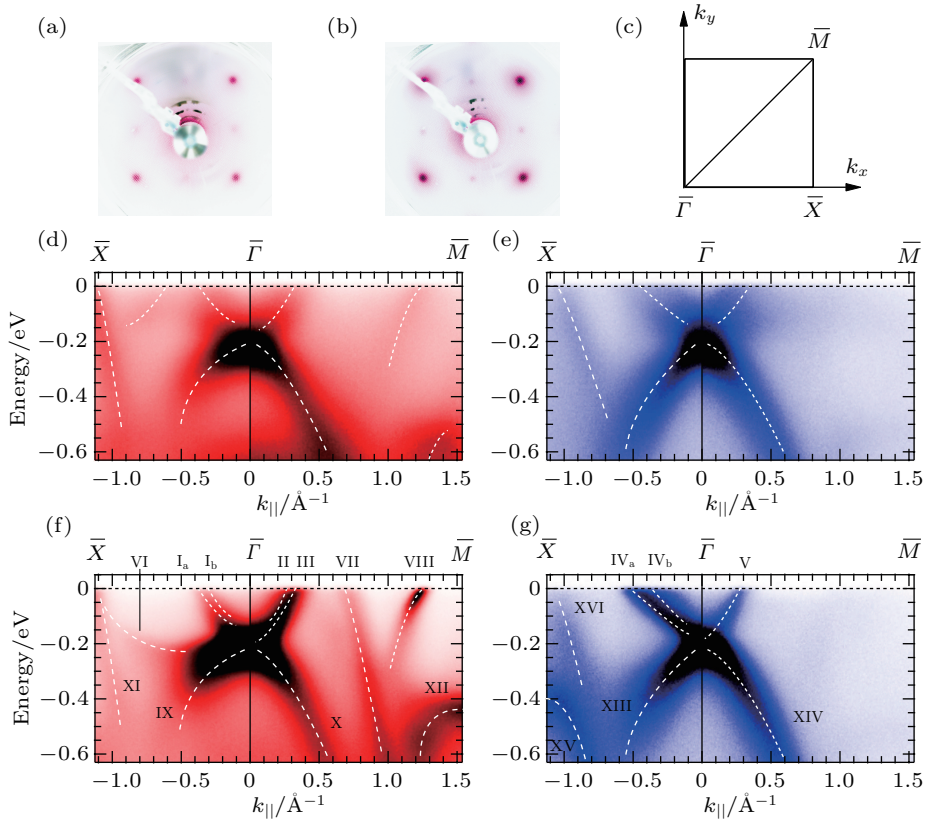


Fig. 1. LEED images of clean Fe(001) (a) and Fe(001)–$p(1 \times 1)$-O (b) taken at the electron kinetic energy of $E_K = 39$ eV. (c) Surface Brillouin zone. The ARPES image plots of clean Fe(001) with the p-polarization geometry (d) and s-polarization geometry (e) taken at $h\nu = 55$ eV. The ARPES image plots of Fe(001)–$p(1 \times 1)$-O with the p-polarization geometry (f) and s-polarization geometry (g) taken at $h\nu = 55$ eV. The dashed lines are guides to the eyes.

Figures 2(a) and 2(b) show the observed Fermi surfaces of pure Fe(001) and Fe(001)–$p(1 \times 1)$-O, respectively, taken within the p (upper panel) and s (lower panel) polarization geometries. In Fig. 2(a), a rounded-square-like Fermi surface exists around the $\overline{\Gamma}$ point in both p- and s-polarization geometries. In the upper half, one can clearly see an arc-like Fermi surface near the $\overline{M}$ point, and there also exist weak features in between the $\overline{\Gamma}$–$\overline{X}$ and $\overline{\Gamma}$–$\overline{M}$ lines. In the lower half, on the other hand, a square-like Fermi surface having a corner at the $\overline{X}$ point can be seen. After oxygen adsorption, in Fig. 2(b), as the linewidth is significantly narrowed, the shape of the Fermi surfaces can be clearly identified. One can see square-like Fermi surfaces surrounding the $\overline{\Gamma}$ point, an arc-shaped Fermi surface near the $\overline{M}$ point, and square-like Fermi surfaces having a corner at the $\overline{X}$ point.

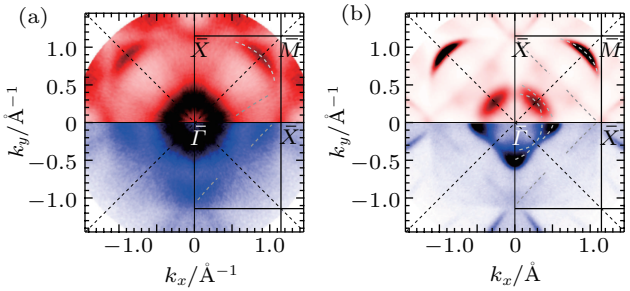


Fig. 2. Fermi surface mappings of clean Fe(001) (a) and Fe(001)–$p(1 \times 1)$-O (b) taken at $h\nu = 55$ eV. The figures in red (top panel) and blue (bottom panel) color scale were taken with the p- and s-polarization geometries, respectively. The dashed lines are guides to the eyes.

As demonstrated in Figs. 1 and 2, significant modifications of the electronic states occur near E_F after the oxygen adsorption. To analyze the p–d hybridization in more detail, we

will compare the results with the layer- and orbital-resolved DFT calculations.

Figure 3(a) shows the ARPES intensity plot and a momentum distribution curve (MDC) at E_F taken with the *p*-polarization geometry. The MDC is the photoemission intensity distribution as a function of $k_{\|}$ at fixed energy. Based on the lineshape analysis of the MDC at E_F, we have evaluated Fermi wave number (k_F) values of the bands. In Fig. 3(a), the electron-like bands I_a and I_b cross E_F at $k_{\|} = 0.36$ Å^{-1} and $k_{\|} = 0.28$ Å^{-1}, respectively. The hole-like band XI crosses E_F near the $\overline{X}$ point.

Figures 3(b)–3(d) show the layer-resolved DFT results for the topmost layer (S), the second layer (S-1), and the layer in the bulk (the central layer of the 41 ML slab). In Figs. 3(b) and 3(c), there exists a surface-derived electron-like state with $k_F = 0.75$ Å^{-1}, corresponding to the bands I_a and I_b in Fig. 3(a). However, the theoretical k_F value is more than two times larger than the observed ones, and there is no splitting as seen in the ARPES results. Furthermore, the observed energy for the bottom of the bands I_a and I_b is about -0.2 eV at the $\overline{\Gamma}$ point while it is about -0.7 eV in the DFT calculation. Taking into account the effective mass enhancement by a factor of 2–3 due to electron correlation for pure Fe,[29,30] one may consider that the observed bands I_a and I_b are elevated towards E_F in the same way. In the present case, however, this explanation is not sufficient as the k_F values clearly differ between experiment and theory. This indicates the change of the Fermi surface volume, namely, change of the carrier density in addition to possible band renormalization effect, which is one of the characteristics of the multi-band electron systems.[41]

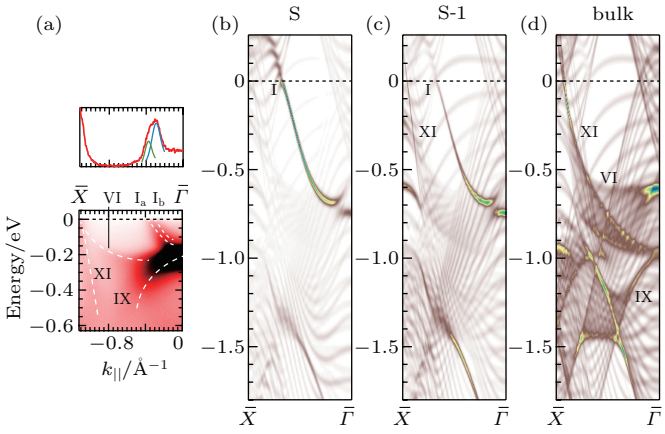


Fig. 3. (a) The experimental ARPES image plot and MDC at E_F of Fe(001)–$p(1\times1)$-O along the $\overline{\Gamma}$–$\overline{X}$ high symmetry line of the surface Brillouin zone taken at $h\nu = 55$ eV with the *p*-polarization geometry. DFT calculation results for (b) the topmost (S), (c) second (S-1), and (d) bulk Fe layers. The dashed lines in (a) are guides for the band dispersions.

To clarify the electronic states in more detail, we compare the ARPES results with the layer- and orbital-resolved DFT calculations relevant for the *p*-polarization geometry along the $\overline{\Gamma}$–$\overline{X}$ line [Figs. 4(a)–4(k)]. One can see that an electron-like band having orbital character of d_{xz} [Figs. 4(a) and 4(b)] and $d_{x^2-y^2}$ [Figs. 4(d) and 4(e)] crosses E_F along the $\overline{\Gamma}$–$\overline{X}$ line, which corresponds to the observed bands I_a and I_b. However, in the DFT calculations, the d_{xz} and $d_{x^2-y^2}$ energies are degenerated along the $\overline{\Gamma}$–$\overline{X}$ line. Note that the d_{xz} contributions from the S and S-1 layers are large near the $\overline{\Gamma}$ point while the $d_{x^2-y^2}$ contribution from the S layer is large near E_F. There are corresponding features in O p_x [near the $\overline{\Gamma}$ point in Fig. 4(j)], p_z [near E_F in Fig. 4(k)], indicating the existence of the p–d hybridization in the surface region. Later, by combining with the results from the *s*-polarization geometry, we will identify the orbital characters of the split energy bands observed in the ARPES.

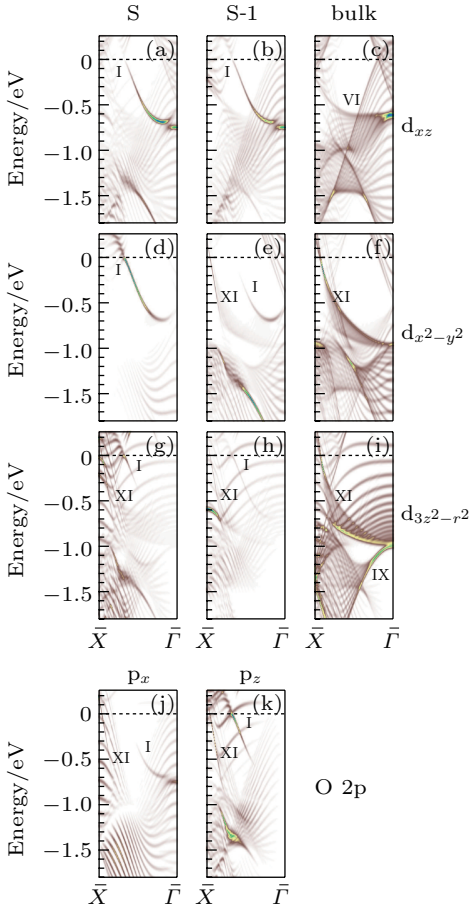


Fig. 4. Layer- and orbital-resolved DFT calculation results of Fe(001)–$p(1\times1)$-O along the $\overline{\Gamma}$–$\overline{X}$ high symmetry line of the surface Brillouin zone. (a)–(c) Fe d_{xz}, (d)–(f) Fe $d_{x^2-y^2}$, (g)–(i) Fe $d_{3z^2-r^2}$, (j) O p_x, and (k) p_z. S and S-1 denote the topmost and second Fe layers for the d orbitals.

The observed band XI corresponds to the $d_{x^2-y^2}$ orbital in the S-1 and bulk layers [Figs. 4(e) and 4(f)] as well as the $d_{3z^2-r^2}$ orbital in the S, S-1 and bulk layers [Figs. 4(g), 4(h) and 4(i)]. The corresponding features in O p_x, p_z [near the $\overline{X}$ point in Figs. 4(j) and 4(k)] indicate the existence of the p–d hybridization in the surface region. The band VI in Fig. 3(a) corresponds to the d_{xz} orbital [Fig. 4(c)] in the bulk and the band IX corresponds to the $d_{3z^2-r^2}$ orbital [Fig. 4(i)] in the

bulk, which is consistent with the absence of the corresponding feature in the oxygen derived states in Figs. 4(j) and 4(k).

Figure 5(a) shows the ARPES intensity plot and the MDC at E_F taken with the *s*-polarization geometry along the $\overline{\Gamma}$–$\overline{X}$ line. Based on the analysis of the MDC, the bands IV_a and IV_b cross E_F at $k_{\parallel} = 0.50$ Å^{-1} and $k_{\parallel} = 0.34$ Å^{-1}, respectively. In Figs. 5(b) and 5(c), the layer-resolved DFT results also show electron-like and hole-like bands centered at the $\overline{\Gamma}$ point corresponding to the bands IV_a/IV_b and XIII. The layer- and orbital-resolved DFT results in Figs. 6(a)–6(f) further reveal that these states are derived from the d_{xy} and d_{yz} orbitals mainly from the S and S-1 layers. The O p_y orbital in Fig. 6(g) also shows features corresponding to the bands IV_a/IV_b and XIII, showing the p–d hybridization near the surface layers. On the other hand, the band XV is derived from the d_{yz} in the S layer [Fig. 6(d)] and d_{xy} in the S-1 layer [Fig. 6(b)] with the negligible p_y contribution. Note that the observed band energy −0.40 eV at the $\overline{X}$ point is much elevated compared with the DFT result −1.73 eV, which corresponds to an effective mass enhancement factor of ∼ 4.

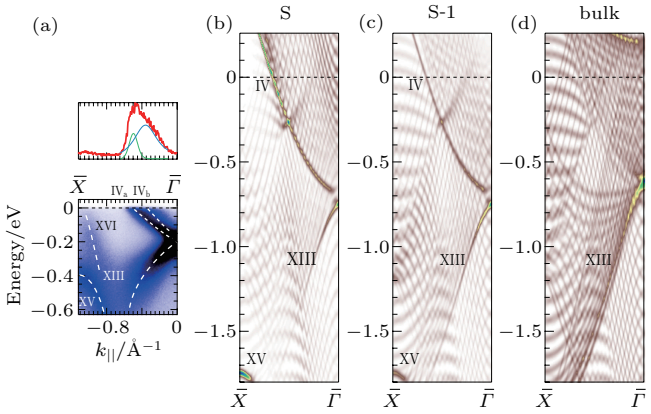


Fig. 5. (a) The experimental ARPES image plot and MDC at E_F of Fe(001)–$p(1\times1)$ along the $\overline{\Gamma}$–$\overline{X}$ high symmetry line of the surface Brillouin zone taken at $h\nu = 55$ eV with the *s*-polarization geometry. DFT calculation results for (b) the topmost (S), (c) second (S-1), and (d) bulk Fe layers. The dashed lines in (a) are guides for the band dispersion.

Here we consider the origin of the split electron-like bands as observed in the ARPES results along the $\overline{\Gamma}$–$\overline{X}$ line taking into account the symmetry properties of the orbitals. We assume the d_{xz}- and d_{yz}-orbital contributions, as observed in the *p*- and *s*-polarization geometries, respectively, should be similar near the $\overline{\Gamma}$ point because they are classified as the Γ_5 of a square lattice at the $\overline{\Gamma}$ point. In this case, we can assign the bands I_a and IV_b having similar k_F values, 0.34–0.36 Å^{-1}, near the $\overline{\Gamma}$ point as derived from the d_{xz} and d_{yz} orbitals, respectively. Then the band I_b at 0.28 Å^{-1} is likely to be derived from the $d_{x^2-y^2}$ (Γ_3) orbital, and the band IV_a at 0.50 Å^{-1} from the d_{xy} (Γ_4) orbital.

Figure 7(a) shows the ARPES intensity plot and MDC at E_F with the *p*-polarization geometry along the $\overline{\Gamma}$–$\overline{M}$ line. Analyses of the MDC at E_F indicate the existence of two electron-like bands II and III crossing E_F at $k_{\parallel} = 0.25$ Å^{-1} and $k_{\parallel} = 0.34$ Å^{-1}, respectively. In Figs. 7(b) and 7(c), the DFT calculations indicate the surface-derived bands corresponding to the bands II and III. In the calculations, these bands cross E_F at $k_{\parallel} = 0.49$ Å^{-1} and $k_{\parallel} = 0.62$ Å^{-1}, which are larger than the observed k_F values though the deviations are slightly smaller than those along the $\overline{\Gamma}$–$\overline{X}$ line (see k_F^{ARPES}/k_F^{DFT} values along $\overline{\Gamma}$–$\overline{X}$ and $\overline{\Gamma}$–$\overline{M}$ lines in Table 1). On the other hand, the Fermi wave number for the band VIII (1.23 Å^{-1}) is slightly larger than the calculation (1.18 Å^{-1}) and that for VII (0.68 Å^{-1}) is close to the theoretical one (0.69 Å^{-1}). These observations suggest that the Fermi surfaces are deformed inhomogeneously depending on the orbital character as well as momentum direction.

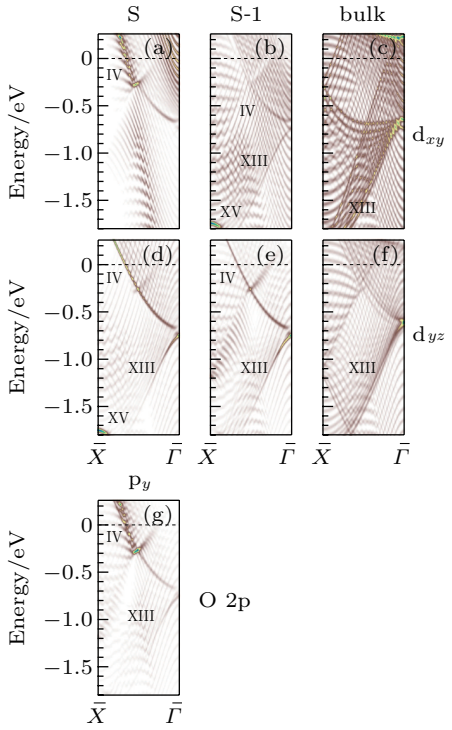


Fig. 6. Layer- and orbital-resolved DFT calculations of Fe(001)–$p(1\times1)$-O (a) near E_F along the $\overline{\Gamma}$–$\overline{X}$ high symmetry line of the surface Brillouin zone. (a)–(c) Fe d_{xy}, (d)–(f) Fe d_{yz}, and (g) O p_y. S and S-1 denote the topmost and second Fe layers for the d orbitals.

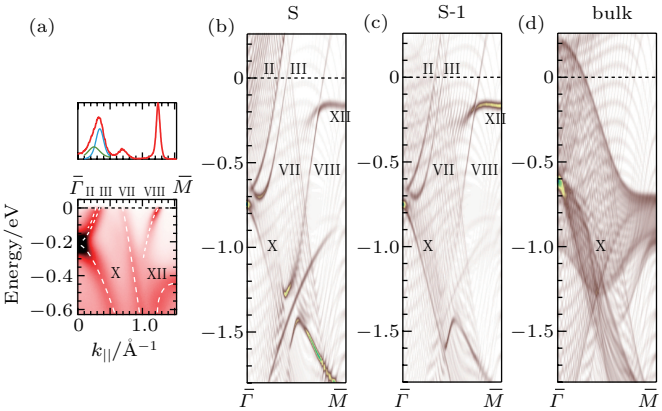


Fig. 7. (a) The experimental ARPES image plot and MDC at E_F of Fe(001)–$p(1\times1)$-O along the $\overline{\Gamma}$–$\overline{M}$ high symmetry line of the surface Brillouin zone taken at $h\nu = 55$ eV with the *p*-polarization geometry. DFT calculation results for (b) the topmost (S), (c) second (S-1) and (d) bulk Fe layers. The dashed lines in (a) are guides for the band dispersions.

In Figs. 8(d) and 8(e), the layer- and orbital-resolved DFT results indicate that the bands Ⅱ and Ⅲ are mainly derived from the $d_{(x+y)z}$ orbital on the S and S-1 layers. The hole-like band X at the $\overline{\Gamma}$ point is either from d_{xy} or $d_{(x+y)z}$ [Figs. 8(b), 8(c), and 8(d)–8(f)]. The corresponding feature exists in the O p_{x+y} orbital [near the $\overline{\Gamma}$ point in Fig. 8(j)], indicating the p–d hybridization. On the other hand, band Ⅶ is derived from the $d_{(x+y)z}$ orbital [Figs. 8(d)–8(f)] and the p_{x+y}, p_z orbitals [Figs. 8(j) and 8(k)]. In the case of band Ⅷ, it corresponds to the d_{xy} and $d_{3z^2-r^2}$ orbitals in the S layer [Figs. 8(a) and 8(g)], and to the $d_{(x+y)z}$ orbital in the S and S-1 layers [Figs. 8(d) and 8(e)]. The corresponding features in the O p_{x+y} and p_z orbitals are weak.

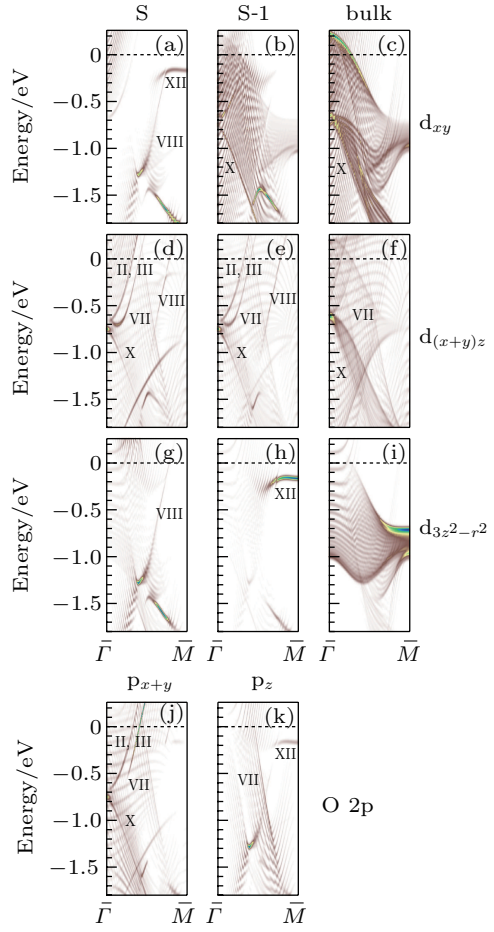


Fig. 8. Layer- and orbital-resolved DFT calculations of Fe(001)–$p(1\times1)$-O along the $\overline{\Gamma}$–$\overline{M}$ high symmetry line of the surface Brillouin zone. (a)–(c) Fe d_{xy}, (d)–(f) Fe $d_{(x+y)z}$, (g)–(i) Fe $d_{3z^2-r^2}$, (j) O p_{x+y}, and (k) O p_z. S and S-1 denote the topmost and second Fe layers for the d orbitals.

The hole-like band XII at the $\overline{M}$ point is mainly derived from the $d_{3z^2-r^2}$ orbital of the S-1 layer [Fig. 8(h)], with a minor contribution from the d_{xy} orbital of the S layer [Fig. 8(a)]. There is a clear corresponding feature in O p_z orbital [Fig. 8(k)], indicating the existence of the p–d hybridization around the $\overline{M}$ point. We should note that the band XII is located at −0.45 eV at the $\overline{M}$ point which is much lower than the theoretical value −0.2 eV, showing a significant contrast to the bands Ⅱ and Ⅲ around the $\overline{\Gamma}$ point having higher energies compared with the DFT results. This observation seems to support our assignment of the band $Ⅳ_a$ as the d_{xy} orbital in the S layer which has larger k_F value compared with the d_{xz}, d_{yz}, and $d_{x^2-y^2}$ orbitals. These results also indicate the interplay of the p–d hybridization and electron correlation depending on the orbital characters.[41]

Figure 9(a) shows the ARPES intensity plot and the MDC at E_F with the *s*-polarization geometry along the $\overline{\Gamma}$–$\overline{M}$ line. Based on the MDC analysis, the band V has the k_F value of 0.28 $Å^{-1}$. As shown in Figs. 9(b) and 9(c), the band V is derived from the $d_{x^2-y^2}$ orbital. The contribution from the S layer is significant compared with that from the S-1 layer. As for the band XIV, however, we could not clearly identify corresponding features in the DFT results. Note that the k_F values for the $d_{x^2-y^2}$ orbital are identical along the $\overline{\Gamma}$–$\overline{X}$ and $\overline{\Gamma}$–$\overline{M}$ lines. While the DFT calculations show a hole-like structure centered at the $\overline{M}$ point in Figs. 9(c) and 9(d), we could not observe the corresponding spectral feature in the ARPES results in the energy range between −0.6 eV and E_F.

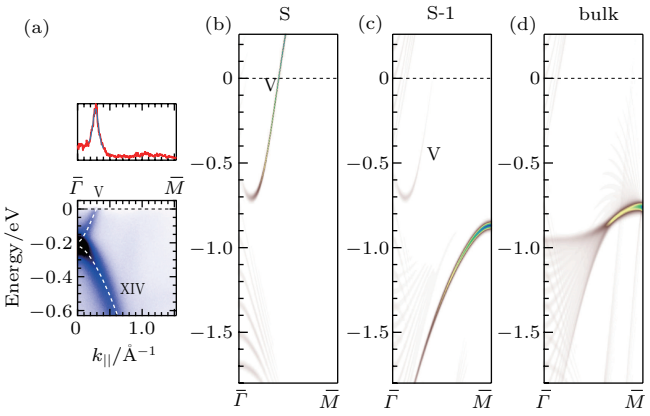


Fig. 9. The experimental ARPES image plot and of Fe(001)–$p(1\times1)$-O (a) near E_F along the $\overline{\Gamma}$–$\overline{M}$ high symmetry line of the surface Brillouin zone taken at $h\nu = 55$ eV with the *s*-polarization geometry. DFT calculation results of the Fe $d_{x^2-y^2}$ orbital component for (b) the topmost (S), (c) second (S-1), and (d) bulk Fe layers. The dashed lines in (a) are guides for the band dispersions.

In Table 1, we summarize the assignment of the orbital character of the observed bands obtained from the detailed comparison between the ARPES results (energy range: −0.6 eV to E_F) and layer- and orbital-resolved DFT calculations. We find the significant p–d hybridization between the Fe d_{xz}, d_{yz}, d_{xy}, $d_{x^2-y^2}$ and O p_x, p_y orbitals in the topmost layer, and the $d_{3z^2-r^2}$ and p_z orbitals in the S-1 layer. These observations are consistent with the symmetry properties of the two-dimensional square lattice[39] as well as previous DFT results.[11] We also find that the bands Ⅵ, Ⅸ, Ⅺ along the $\overline{\Gamma}$–$\overline{X}$ line, and Ⅷ, Ⅴ along the $\overline{\Gamma}$–$\overline{M}$ line are weakly hybridized with the adsorbed oxygen.

Table 1. Orbital character of the observed bands. S, S-1, B denote the topmost, second, and bulk Fe layers, respectively. $k_{\rm F}^{\rm ARPES}$ and $k_{\rm F}^{\rm DFT}$ in units of Å^{-1} represent the Fermi wave number obtained from the ARPES and DFT results, respectively.

Direction	Polarization	Band	Fe orbital (layer)	O orbital	$k_{\rm F}^{\rm ARPES}$	$k_{\rm F}^{\rm DFT}$	$k_{\rm F}^{\rm ARPES}/k_{\rm F}^{\rm DFT}$
$\overline{\Gamma}$–$\overline{X}$	p	$\rm I_a$	d_{xz} (S, S-1)	p_x, p_z	0.36	0.75	0.48
	p	$\rm I_b$	$d_{x^2-y^2}$ (S, S-1)	p_x, p_z	0.28	0.75	0.37
	p	VI	d_{xz} (B)	–			
	p	IX	$d_{3z^2-r^2}$ (B)	–			
	p	XI	$d_{x^2-y^2}$ (S-1,B), $d_{3z^2-r^2}$ (S,S-1,B)	p_x, p_z			
	s	$\rm IV_a$	d_{xy} (S, S-1)	p_y	0.50	0.74	0.68
	s	$\rm IV_b$	d_{yz} (S, S-1)	p_y	0.34	0.74	0.46
	s	XIII	d_{yz} (S,S-1,B), d_{xy} (S-1,B)	p_y			
	s	XV	d_{yz} (S), d_{xy} (S-1)	–			
	s	XVI	d_{xy} (S)?	–			
$\overline{\Gamma}$–$\overline{M}$	p	II, III	$d_{(x+y)z}$ (S, S-1)	p_{x+y}	0.25, 0.34	0.49, 0.62	0.51, 0.55
	p	VII	$d_{(x+y)z}$ (S, S-1, B)	p_{x+y}, p_z	0.68	0.69	0.99
	p	VIII	$d_{3z^2-r^2}$ (S), d_{xy} (S), $d_{(x+y)z}$ (S, S-1)	–	1.23	1.18	1.04
	p	X	$d_{(x+y)z}$ (S, S-1, B), d_{xy} (S-1, B)	p_{x+y}			
	p	XII	d_{xy} (S), $d_{3z^2-r^2}$ (S-1)	p_z			
	s	V	$d_{x^2-y^2}$ (S,S-1)	–	0.28	0.62	0.45
	s	XIV	$d_{x^2-y^2}$ (S,S-1,B)?	–			

Finally it should be emphasized that the electron-like bands I–V near the $\overline{\Gamma}$ point are shifted to a higher energy compared with the DFT calculations, while the energy of band XII is shifted downwards. The theoretical $k_{\rm F}$ values for the electron-like Fermi surfaces around the $\overline{\Gamma}$ point are larger than the observed $k_{\rm F}$ values, and the magnitudes of the deviation depend on the orbital character and momentum direction. These observations indicate the significance of the anisotropic interplay of electron correlation and p–d hybridization in the multi-band low-dimensional electron system.

6. Conclusion

We have studied the electronic states of clean Fe(001) and Fe(001)–$p(1\times1)$-O films grown on MgO(001) substrates near $E_{\rm F}$ in the surface region by means of polarization-dependent ARPES measurements and extensive DFT calculations. We have observed significant modifications of the energy bands and the Fermi surfaces induced by the oxygen adsorption. Based on the detailed comparison between the ARPES results and DFT calculations, we have found the orbital-dependent p–d hybridization in the topmost and second Fe layers. We have also found that the observed band energy and $k_{\rm F}$ values are deviated from the DFT calculations depending on the orbital characters and momentum directions. It clearly indicates the anisotropic interplay of the electron correlation and p–d hybridization effects near the surface region. Our results have provided a comprehensive view of the electronic states near $E_{\rm F}$ of the oxygen adsorbed Fe(001) surface as well as insight into electron correlation in the multi-band low-dimensional electron system.

Acknowledgments

We thank N-BARD, Hiroshima University for supplying the liquid helium. The synchrotron radiation experiments were performed with the approval of program advisory committee of HiSOR (Proposals Nos. 13-A-39, 14-A-51, 14-A-52, 15-A-64, 16AG038, 17AG051). Z.M. acknowledges financial support from the China Scholarship Council. E.F.S acknowledges financial support from the JSPS postdoctoral fellowship for overseas researchers as well as the Alexander von Humboldt Foundation (Grant No. P13783). We thank Prof. Taichi Okuda and Prof. Koji Miyamoto for the helpful information on the preparation of Fe(001)–$p(1\times1)$-O surface.

References

[1] Henrich V E and Cox P A 1994 *The surface science of metal oxides* (Cambridge: Cambridge University Press)
[2] Parkinson G S 2016 *Surf. Sci. Rep.* **71** 272
[3] Uebing C 1998 *Prog. Solid. State Ch.* **26** 155
[4] Picone A, Riva M, Brambilla A, Calloni A, Bussetti G, Finazzi M, Ciccacci F and Duò L 2016 *Surf. Sci. Rep.* **71** 32
[5] Yuasa S, Nagahama T, Fukushima A, Suzuki Y and Ando K 2004 *Nature Mater.* **3** 868
[6] Fu Q, Li W X, Yao Y, Liu H, Su H Y, Ma D, Gu X K, Chen L, Wang Z, Zhang H, Wang B and Bao X 2010 *Science* **328** 1141
[7] Legg K O, Jona F, Jepsen D W and Marcus P M 1977 *Phys. Rev. B* **16** 5271
[8] Jona F and Marcus P M 1987 *Solid State Commun.* **64** 667
[9] Headrick R L, Konarski P, Ylisove S M and Graham W R 1989 *Phys. Rev. B* **39** 5713
[10] Parihar S S, Meyerheim H L, Mohseni K, Ostanin S, Ernst A, Jedrecy N, Felici R and Kirschner J 2010 *Phys. Rev. B* **81** 075428
[11] Huang H and Hermanson J 1985 *Phys. Rev. B* **32** 6312
[12] Chubb S R and Pickett W E 1987 *Phys. Rev. Lett.* **58** 1248
[13] Błoński P, Kiejna A and Hafner J 2005 *Surf. Sci.* **590** 88
[14] Błoński P, Kiejna A and Hafner J 2007 *J. Phys.: Condens. Matter* **19** 096011
[15] Hugosson H W, Cao W M, Seetharaman S and Delin A 2013 *J. Phys. Chem. C* **117** 6161
[16] Panzner G, Mueller D R and Rhodin T N 1985 *Phys. Rev. B* **32** 3472

[17] Johnson P D, Clarke A, Brookes N B, Hulbert S L, Sinkovic B and Smith N V 1988 *Phys. Rev. Lett.* **61** 2257

[18] Clarke A, Brookes N B, Johnson P D, Weinert M, Sinkovic B and Smith N V 1990 *Phys. Rev. B* **41** 9659

[19] Fink R L, Mulhollan G A, Andrews A B, Erskine J L and Walters G K 1992 *Phys. Rev. B* **45** 9824

[20] Eibl C, Schmidt A B and Donath M 2012 *Phys. Rev. B* **86** 161414

[21] Donati F, Sessi P, Achilli S, Li Bassi A, Passoni M, Casari C S, Bottani C E, Brambilla A, Picone A, Finazzi M, Duò L, Trioni M I and Ciccacci F 2009 *Phys. Rev. B* **79** 195430

[22] Picone A, Fratesi G, Brambilla A, Sessi P, Donati F, Achilli S, Maini L, Trioni M I, Casari C S, Passoni M, Li Bassi A, Finazzi M, Duò L and Ciccacci F 2010 *Phys. Rev. B* **81** 115450

[23] Picone A, Brambilla A, Calloni A, Duò L, Finazzi M and Ciccacci F 2011 *Phys. Rev. B* **83** 235402

[24] Tange A, Gao C L, Yavorsky B Y, Maznichenko I V, Etz C, Ernst A, Hergert W, Mertig I, Wulfhekel W and Kirschner J 2010 *Phys. Rev. B* **81** 195410

[25] Bertacco R and Ciccacci F 1999 *Phys. Rev. B* **59** 4207

[26] Bertacco R, Merano M and Ciccacci F 1998 *Appl. Phys. Lett.* **72** 2050

[27] Bertacco R, Onofrio D and Ciccacci F 1999 *Rev. Sci. Instrum.* **70** 3572

[28] Okuda T, Takeichi Y, Maeda Y, Harasawa A, Matsuda I, Kinoshita T and Kakizaki A 2008 *Rev. Sci. Instrum.* **79** 123117

[29] Schäfer J, Hoinkis M, Rotenberg E, Blaha P and Claessen R 2005 *Phys. Rev. B* **72** 155115

[30] Cui X Y, Shimada K, Sakisaka Y, Kato H, Hoesch M, Oguchi T, Aiura Y, Namatame H and Taniguchi M 2010 *Phys. Rev. B* **82** 195132

[31] http://www.openmx-square.org

[32] Ceperley D M and Alder B J 1980 *Phys. Rev. Lett.* **45** 566

[33] http://www.openmx-square.org/openmx_man3.8/node153.html

[34] Popescu V and Zunger A 2012 *Phys. Rev. B* **85** 085201

[35] Mulliken R S 1955 *J. Chem. Phys.* **23** 1833

[36] Shimada K, Arita M, Matsui T, Goto K, Qiao S, Yoshida K, Taniguchi M, Namatame H, Sekitani T, Tanaka K, Yoshida H, Shirasawa K, Smolyakov N and Hiraya A 2001 *Nucl. Instrum. Methods Phys. Res. A* **467–468** 504

[37] Iwasawa H, Shimada K, Schwier E F, Zheng M, Kojima Y, Hayashi H, Jiang J, Higashiguchi M, Aiura Y, Namatame H and Taniguchi M 2017 *J. Synchrotron Rad.* **24** 836

[38] Taking into account the ARPES results on pure Fe(001) given by Plucinski *et al.* 2009 *Phys. Rev. B* **80** 184430, the inner potential V_0 is estimated to be $|V_0| \sim 6$–7 eV. In this case, the k_z value for the ARPES result taken at $h\nu = 55$ eV is away from the Γ point about $\sim 25\%$ of the distance between Γ and H points of the bulk Brillouin zone. Hence it is closer to the Γ point.

[39] Kittel C 1987 *Quantum theory of solids*, 2nd Edn. (New York: John Wiley & Sons)

[40] Callaway J and Wang C S 1977 *Phys. Rev. B* **16** 2095

[41] Liebsch A and Lichtenstein A 2000 *Phys. Rev. Lett.* **84** 1591